Millimeter Wave Massive MIMO beamforming communication simulator design: a systematic approach

A Thesis Presented
by

Zhengnan Li

to

The Department of Electrical and Computer Engineering

in partial fulfillment of the requirements
for the degree of

Master of Science

in

Electrical and Computer Engineering

Northeastern University
Boston, Massachusetts

July 2018

To my family – without whom I would not have the chance of seeing a better world.

To my friends during masters' – Amanda, Spark, Mingyu, Ken, for your generous support throughout.

To Tiansu – happy belated birthday, and sincerely wish you the best in your endeavors.

Contents

List of Figures

List of Tables

Acronyms

3GPP	3^{rd} Generation Partnership Project.
AGC	Automatic Gain Control.
AoA	Azimuth angle of Arrival.
AoD	Azimuth angle of Departure.
AP	Access Point.
ASA	Azimuth angle Spread of Arrival.
ASD	Azimuth angle Spread of Depature.
AWGN	Additive White Gaussian Noise.
AWV	Antenna Weight Vector.
BF	Beamforming Field.
CA	Carrier Sensing.
CCA	Clear Channel Assessment.
CDL	Clustered Delay Line.
CEF	Channel Estimation Field.
CIR	Channel Impluse Response.
DF	Data Field.
DMG	Directional multi-gigabit.
DoA	Direction of Arrival.
DoF	Degree of Freedom.
FDE	Frequency Domain Equalization.
FIR	Finite Impulse Response.
GCS	Global Coordinate System.
LCMV	Linear-Constrained Minimum Variance.
LCS	Local Coordinate System.
LDPC	Low Density Parity Check.
LoS	Line of Sight.
LUT	Look Up Table.

MAC	Medium Access Control Layer.
MCS	Modulation and Coding Scheme.
MIMO	Multiple Input Multiple Output.
ML	Maximum Likelihood.
MPC	MultiPath Cluster.
MSE	Mean Squared Error.
MVDR	Minimum Variance Distortionless Response.
NLoS	Non Line of Sight.
OFDM	Orthogonal Frequency-Division Multiplexing.
PDP	Power Delay Profile.
PER	Packet Error Rate.
PHY	Physical Layer.
PPDU	PLCP Protocol Data Unit.
PSDU	PLCP Service Data Unit.
QoS	Quality of Service.
RMS	Rooted Mean Square.
RSS	Received Signal Strength.
SC	Single Carrier.
SNR	Signal to Noise Ratio.
STA	Station.
STF	Short Training Field.
TRN-T/R	Training Field (Transmit/Receive).
ULA	Uniform Linear Array.
XPR	Cross Polarization Ratio.
ZoA	Zenith angle of Arrival.
ZoD	Zenith angle of Departure.
ZSA	Zenith angle Spread of Arrival.
ZSD	Zenith angle Spread of Depature.

Acknowledgments

I would like to express my gratitude to my advisor Prof. Chowdhury for his generous support, his encouragement throughout my master's study, and patience in guiding me on technical issues. His academical excellence, his dedication, and his passion for research will always enlighten me furthering my studies in wireless communications.

I would also like to thank all my colleagues both in lab and at the MathWorks – Miad, Parisa, Munish, Amir, Yashar, Stella, Kunal, and Mike, Ethem, Tasos, Yue – without your help and guidance this work wouldn't finish. It is always my pleasure to exchange ideas with you and those ideas always shine. Besides, thanks to Haoran, Wangbo, Ruixiao on their supports.

Special thanks to Prof. Stojanovic, from whom I learn how to be a researcher and a positive observer.

Abstract of the Thesis

Millimeter Wave Massive MIMO beamforming communication simulator design: a systematic approach

by

Zhengnan Li

Master of Science in Electrical and Computer Engineering

Northeastern University, July 2018

Dr. Kaushik R. Chowdhury, Advisor

With the growth of data traffic demands, wireless network architectures that use traditional sub-6 GHz frequency bands are now reaching their capacities. Millimeter wave (mmWave) communication is a transformative paradigm given its potential to attain throughput that goes beyond several gigabits per second, with over 2-4GHz of bandwidth. However, it also incurs high levels of signal attenuation that raises challenges in connectivity with increasing distance. The relatively high pathloss can be mitigated via beamforming technique, where signal energy is directed towards a specific user or target by appropriately weighting the phases of the antenna elements. In addition, the comparatively small millimeter wavelength also allows practicability of employing massive antenna elements within a small surface area. Thus, so called 'massive' clusters of antenna elements are now possible. This thesis presents a systematic simulator design for mmWave-based network architectures, fulfilling the requirements of next generation of telecommunication (5G).

In this thesis, a beamforming enabled massive multiple input multiple output (MIMO) based physical (PHY) layer simulator design is proposed and implemented in MATLAB. It consists of IEEE 802.11ad standard compliant transceiver design, 3GPP TR 38.901 channel model, and beamforming performance evaluation platform. The simulator facilitates assessment of different beamforming algorithms, as well as Medium Access Control (MAC) layer design process. Along with the transceiver, a Modulation and Coding Scheme (MCS) selection mechanism is also proposed to guarantee timing and throughput requirements from upper layer. Packet Error Rate (PER) results of the transceiver is simulated with different Clustered Delay Line (CDL) profiles suggested by TR 38.901.

Chapter 1

Introduction

With the growth of data traffic in cellular networks, and more demanding Quality of Service (QoS) requirements, traditional sub-6 GHz system capacities are prone to reach their maximum. Millimeter wave communications [1] are emerging recently, with its advantages in higher bandwidth and throughput, gradually adapted in next generation of communications.

However, pathloss grows exponentially with frequency – thus omnidirectional antenna communication suffers a lot in Signal to Noise Ratio (SNR). Combining beamforming technology along with mmWave is promising [2] because the wavelength of mmWave is millimeter, and the implementation of massive Multiple Input Multiple Output (MIMO) can be limited into reasonable size – this has been experimentally verified in [3]. Large antenna arrays are capable of providing beamforming gain to achieve reasonable SNR. However, traditional beamforming which has all antenna connected with individual RF chain and dedicated baseband process is not appropriate in mmWave communication because the number of antenna in mmWave massive MIMO may reach 128 or even more – this brings the issues with cost and power efficiency. Hybrid beamforming – which combines analog beamformer (phase shifters) and digital beamformer (individual RF chain) – has drawn more and more attention [4]. Generally speaking, to solve the power and cost constraints in massive mmWave MIMO systems, studies focuses on (i) uses phase shifters, as in [5], [6] which multiply a simple constraint on antenna elements; (ii) antenna selection, which considers a subset of antenna array thus replaces the phase shifters by even simpler analog switches, like in [7], and their capacities [8].

Regarding mmWave communication band and protocol, in the frequency range around 60 GHz, multiple unlicensed bands are available globally. For example, The European Union dedicated 57 - 66 GHz band to unlicensed band, and USA uses 55.05 - 64 GHz band, providing massive

opportunities of achieving multi-gigabit transmission rate. However, the primary challenge with 60GHz band communication is that the pathloss is much poorer than those in the sub-6 GHz bands – the free-space pathloss at 1m for 60 GHz is 68dB whereas 47 dB at 5 GHz. The IEEE 802.11ad protocol [9] uses a so called Directional multi-gigabit (DMG) packet, whose aim is to beamform towards desired direction to provide gigabyte bandwidth communication link. The DMG Physical Layer (PHY) supports three modulation methods, a control modulation using Modulation and Coding Scheme (MCS) 0; a single carrier modulation using MCS 1 to MCS 12; and an Orthogonal Frequency-Division Multiplexing (OFDM) modulation using MCS 13 to MCS 25. This paper will focus on Single Carrier (SC) 802.11ad communication link simulations.

To simulate a complete communication link, the channel between transmitter and receiver is required. The 3^{rd} Generation Partnership Project (3GPP) released a technical report, named Study on Channel Model for Frequencies from 0.5 to 100GHz, labeled 3GPP TR 38.901 [10], described and summarized a systematic method in modeling and evaluate the performance of physical layer techniques, by simulating the radio channel. This model suggests series of key parameters describing a relative complete scenario, from pathloss to large scale fading, reaching finally at small scale parameters.

Finally, this thesis presents a massive MIMO mmWave beamforming communication link simulator, by introducing its components in the following chapter, namely, 802.11ad PHY introduction, 3GPP TR 38.901 channel model summarization, 802.11ad PHY receiver reference design and its Packet Error Rate (PER) performance, introduction to beamforming, and the last chapter states the integrated simulator design.

The main contribution of this thesis lies in the proposed integrated beamforming-communication simulator, for its usages in beamforming algorithm evaluation, mmWave PHY/Medium Access Control Layer (MAC) layer co-design etc. This thesis first presents the PER results under different 3GPP TR 38.901 channel model Clustered Delay Line (CDL) profiles, and then presents the PER results of different beamformers to demonstrate their performance.

Chapter 2

Introduction to 802.11ad Physical Layer

2.1 802.11ad Single Carrier PHY Frame Format

As shown in Figure 2.1, the single carrier PHY contains several fields, itemizing,

- Short Training Field (STF) is composed of 16 repetitions of Golay sequences of length 128, $Ga_{128}(n)$, followed by a single repetition of $-Ga_{128}(n)$.
- Channel Estimation Field (CEF) is used for channel estimation and the indication of modulation. The CEF composes two sequences, $Gu_{512}(n)$ and $Gv_{512}(n)$, where $Gu_{512} = [-Gb_{128}, -Ga_{128}, Gb_{128}, -Ga_{128}]$, and $Gv_{512} = [-Gb_{128}, Ga_{128}, -Gb_{128}, -Ga_{128}]$. Note that Gb_{128} is also a Golay sequence of length 128. For single carrier packets, the format of this channel estimation field is different from that in OFDM packet. Because of the good autocorrelation property of the Golay sequence, it enables the reconstruction of Channel Impluse Response (CIR) between the transmitter and the receiver – a summation of autocorrelations of Ga_{128} and Gb_{128} is the Dirac delta function – naturally formulates CIR.
- Header consists of several fields that define of the details of PLCP Protocol Data Unit (PPDU) to be transmitted later, e.g., MCS, length of PPDU etc.
- Data Field (DF) composes the payload data of the PLCP Service Data Unit (PSDU) and possible padding. The data after padding with zeros are then scrambled, encoded, and modulated as dictated by MCS, the modulation and coding scheme. The scrambler uses a polynomial $S(x) = x^7 + x^4 + 1$, generating a periodic sequence of length 127. The data are then encoded by a systematic Low Density Parity Check (LDPC) encoder.

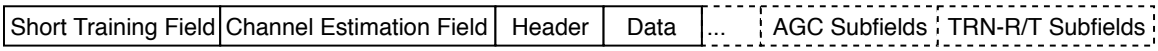

Figure 2.1: SC PHY frame format

- (Optional) Beamforming Field (BF), including Automatic Gain Control (AGC) field, and Training Field (Transmit/Receive) (TRN-T/R). Beamforming enables both Tx-Rx side to train their transmit and receive antenna for better communication conditions (power). In the AGC field, it composes several repetitions of Golay sequence. The TRN-T/R field consists Golay sequence, but applied with different Antenna Weight Vector (AWV) to beamform towards different direction.

2.2 Common parameters and requirements for 802.11ad

The following section lists several parameters and requirements for transceivers,

- Receiver sensitivity, for MCS 0, the PER shall be less than 5% for a PSDU length of 256 bytes, and less than 1% for other MCSs with a PSDU length of 4096 octets, depending their corresponding input levels.
- Timing related parameters. Table 2.1 states part of timing-related constants of 802.11ad protocol. Note that this table contains parameters describing SC PHY.

Parameter	Value
F_c: SC chip rate	1760 MHz
T_c: SC chip time	$0.57ns = 1/F_c$
T_{seq}	$72.7ns = 128 \times T_c$
T_{STF}: short training field duration	$1236ns = 17 \times T_{seq}$
T_{CE}: channel estimation field duration	$655ns = 9 \times T_{seq}$
T_{HEADER}: header duration	$0.582\mu s = 2 \times \times T_c$
T_{Data}	$(N_{BLKS} \times 512 + 64) \times T_c$

Table 2.1: (Part of) Timing-related parameters of 802.11ad

Note that the N_{BLKS} is the number of symbol blocks in the procedure of LDPC encoding.

Chapter 3

Introduction to 3GPP Technical Report 38.901 Channel Models

The following steps are required in simulation such channel, namely,

3.1 Methodology in Generating Channel Coefficients

3.1.1 Set environment, network layout and antenna array parameters

- Set simulation environment, e.g., rural outdoor area.
- Set the number of Access Point (AP) and Station (STA).
- Give 3D location, antenna pattern, and array orientations of the AP and STA.
- Give STA's speed and direction of motion
- Specify system center frequency and sample rate according to 802.11ad protocol, here the center frequency of 802.11ad is 60.48 GHz, and the sample rate is 1760 MSa/s

3.1.2 Set (Non) Line of Sight probability and pathloss

- Assign propagation conditions, meaning to set Line of Sight (LoS) or Non Line of Sight (NLoS) uncorrelated conditions to each AP-STA pairs, based on simulation scenario. In this simulator, we assume indoor mixed office setting, and the LoS probability is stated in Equation 3.1,

$$P_{\text{LoS}} = \begin{cases} 1, & d_{2D} \leq 1.2m \\ \exp\left(-\frac{d_{2D}-1.2}{4.7}\right), & 1.2m < d_{2D} < 6.5m \\ \exp\left(-\frac{d_{2D}-6.5}{32.6}\right), & 6.5m < d_{2D} \end{cases} \tag{3.1}$$

The method of determining LoS or NLoS is by generating a uniformly distributed number in [0, 1], if this number is less than P_{LoS}, then we claim this pair of AP-STA is of LoS condition.

- Calculate pathloss for each AP-STA link to be modeled, by Equation 3.2, of the LoS pathloss

$$PL_{\text{In-LoS}}(dB) = 32.4 + 17.3\log_{10}(d_{3D}) + 20\log_{10}(f_c) + \Delta g_{\text{LoS}}, 1m \leq d_{3D} \leq 100m \tag{3.2}$$

where Δg_{LoS} conforms log-normal distribution with 0 mean, 3 dB variance.

For NLoS conditions, they are stated in Equation 3.3,

$$PL_{\text{In-NLoS}}(dB) = \max\left\{PL_{\text{In-LoS}}, PL'_{\text{In-NLoS}}\right\} \tag{3.3}$$

where,

$$PL'_{\text{In-NLoS}} = 38.3\log_{10}(d_{3D}) + 17.30 + 24.9\log_{10}(f_c) + \Delta g_{\text{NLoS}}, 1m \leq d_{3D} \leq 86m \tag{3.4}$$

Δg_{NLoS} conforms log-normal distribution with 0 mean, 8.03 dB variance.

Figure 3.1 shows the pathloss vs. distance plot. The shaded area represents for large-scale shadowing standard deviation range. From this figure we can observe that the LoS is better than NLoS cases, and the higher frequency, more attenuation.

3.1.3 Set small-scale parameters, including delay spread, angular spreads, cross polarization ratio, cluster delays, powers, arrival and departure angle

A CDL profile generally describes power, delay, angles for each clusters. As tabulated in Table 3.1, CDL-C profile describes a LoS scenario, with 23 different clusters, and their corresponding,

- Normalized Delay, scaled by delay spread, i.e.,

$$\tau_{\text{scaled}} = \tau_{\text{model}} \times DS_{desired} \tag{3.5}$$

In this simulation, we uses $16ns$ as the delay spread, recommended by [10] for indoor office, normal-delay profile.

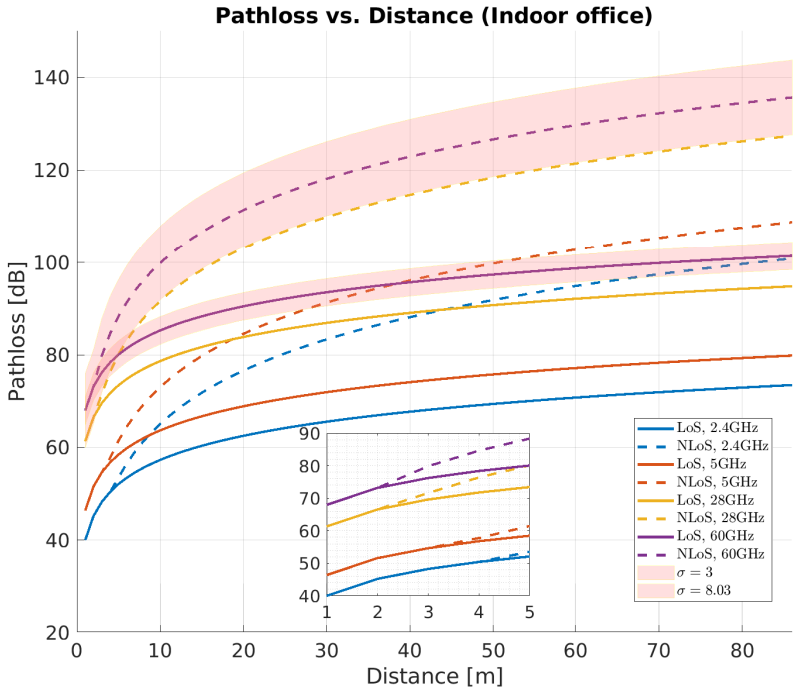

Figure 3.1: Pathloss vs Distance (Indoor office)

- Cluster Power, described in dB (W). Note that for LoS profiles (CDL-D, CDL-E), no scaling of K-factor is applied, so the cluster power is directly from the Power Delay Profile (PDP).

- Azimuth angle of Arrival (AoA) ϕ_{AoA}, Azimuth angle of Departure (AoD) ϕ_{AoD}, Zenith angle of Arrival (ZoA) θ_{ZoA}, Zenith angle of Departure (ZoD) θ_{AoD} of corresponding cluster center and cluster-wise Rooted Mean Square (RMS) angles (c_{ASA} etc.), describing how diverge within angles of that cluster. Then these two set of parameters are used to generate paths within one cluster by Equation 3.6

$$\phi_{n,m,\text{AoA}} = \phi_{n,\text{AoA}} + c_{\text{ASA}}\alpha_m \tag{3.6}$$

where, $\phi_{n,m,\text{AoA}}$ represents path n within cluster m's Azimuth of angle of Arrival, $\phi_{n,\text{AoA}}$ represents the cluster center's AoA, and c_{ASA} is the cluster-wise RMS Azimuth angle Spread of Arrival (ASA), and α_m is denotes the ray offset angles within a cluster for path m, for example, path number 1 ($m = 1$), the basis vector of offset angles α_1 = 0.0447, meaning the first path is 0.0447 radian deviating from the cluster center. Same logic applies for AoD-Azimuth angle

Spread of Depature (ASD), ZoA-Zenith angle Spread of Arrival (ZSA), ZoD-Zenith angle Spread of Depature (ZSD).

- Cross Polarization Ratio (XPR), used to describe the power ratios for each path in each cluster if certain cluster is of NLoS

3.1.4 Draw initial phases and generate channel coefficients

After modeling all above parameters of MultiPath Cluster (MPC), the NLoS channel of the n-th path within cluster $m \in [1, M]$, between the u-th AP antenna and the s-th STA antenna is then given by,

$$H_{u,s,n}^{\text{NLoS}}(t) = \sqrt{\frac{P_n}{M}} \sum_{m=1}^{M} \mathcal{F}_{u,n,m}^{\text{NLoS}} \mathcal{R}_{u,n,m} \mathcal{T}_{s,n,m} \mathcal{D}_{n,m}(t) \tag{3.7}$$

for LoS,

$$H_{u,s,n}^{\text{LoS}}(t) = \sqrt{\frac{P_n}{M}} \sum_{m=1}^{M} \mathcal{F}_{u,n,m}^{\text{LoS}} \mathcal{R}_{u,n,m} \mathcal{T}_{s,n,m} \mathcal{D}_{n,m}(t) \tag{3.8}$$

where,

- P_n is n-th path's power
- $\mathcal{F}_{u,n,m}^{\text{NLoS}}$ stands for the field term of Equation 3.7, including receive antenna patterns $F_{rx,u,\theta}$ and $F_{rx,u,\phi}$, and transmit antenna patterns $F_{tx,u,\theta}$ and $F_{tx,u,\phi}$, with their respects to directions of θ and ϕ (the base spherical vectors) given in Global Coordinate System (GCS) [10]. $\Phi_{n,m}^{\phi\theta}$,$\Phi_{n,m}^{\phi\phi}$ $\Phi_{n,m}^{\theta\theta}$ $\Phi_{n,m}^{\theta\phi}$ are random initial phases for each path m of each cluster n, $\kappa_{n,m} = 10^{X/10}$, X is the XPR, differs from CDL profile to profile.

$$\mathcal{F}_{u,n,m}^{\text{NLoS}} = \begin{bmatrix} F_{rx,u,\theta}(\theta_{n,m,\text{ZoA}}, \phi_{n,m,\text{AoA}}) \\ F_{rx,u,\phi}(\theta_{n,m,\text{ZoA}}, \phi_{n,m,\text{AoA}}) \end{bmatrix}^{\top} \cdot \begin{bmatrix} \exp(j\Phi_{n,m}^{\theta\theta}) & \sqrt{\kappa_{n,m}^{-1}} \exp(j\Phi_{n,m}^{\theta\phi}) \\ \sqrt{\kappa_{n,m}^{-1}} \exp(j\Phi_{n,m}^{\phi\theta}) & \exp(j\Phi_{n,m}^{\phi\phi}) \end{bmatrix} \cdot \begin{bmatrix} F_{tx,s,\theta}(\theta_{n,m,\text{ZoD}}, \phi_{n,m,\text{AoD}}) \\ F_{tx,s,\phi}(\theta_{n,m,\text{ZoD}}, \phi_{n,m,\text{AoD}}) \end{bmatrix} \tag{3.9}$$

- $\mathcal{R}_{u,n,m}$ denotes receive location term, $\hat{\mathbf{r}}_{rx,n,m}$ is the spherical unit vector with arrival angles, stated in Equation 3.10, $\bar{\mathbf{d}}_{rx,u} \in \mathbb{R}^{3\times 1}$ is the location vector of receive antenna element u, and λ_0 is carrier wave length,

$$\mathcal{R}_{u,n,m} = \exp\left(\frac{j2\pi\hat{\mathbf{r}}_{rx,n,m}^{\top}\bar{\mathbf{d}}_{rx,u}}{\lambda_0}\right), \hat{\mathbf{r}}_{rx,n,m} = \begin{bmatrix} \sin\theta_{n,m,\text{ZoA}}\cos\phi_{n,m,\text{AoA}} \\ \sin\theta_{n,m,\text{ZoA}}\sin\phi_{n,m,\text{AoA}} \\ \cos\theta_{n,m,\text{ZoA}} \end{bmatrix} \tag{3.10}$$

- $\mathcal{T}_{s,n,m}$ represents transmit location term, $\hat{\mathbf{r}}_{rx,n,m}$ is the spherical unit vector with departure angles, stated in Equation 3.11, $\bar{\mathbf{d}}_{tx,s} \in \mathbb{R}^{3\times 1}$ is the location vector of transmit antenna element s,

$$\mathcal{T}_{s,n,m} = \exp\left(\frac{j2\pi\hat{\mathbf{r}}_{tx,n,m}^{\top}\bar{\mathbf{d}}_{tx,s}}{\lambda_0}\right), \hat{\mathbf{r}}_{tx,n,m} = \begin{bmatrix} \sin\theta_{n,m,\text{ZoD}}\cos\phi_{n,m,\text{AoD}} \\ \sin\theta_{n,m,\text{ZoD}}\sin\phi_{n,m,\text{AoD}} \\ \cos\theta_{n,m,\text{ZoD}} \end{bmatrix} \tag{3.11}$$

- $\mathcal{D}_{n,m}(t)$ indicates the Doppler term, $\bar{\mathbf{v}}$ is the STA velocity with speed v, along azimuth angle ϕ_v and elevation angle θ_v,

$$\mathcal{D}_{n,m}(t) = \exp\left(j2\pi\hat{\mathbf{r}}_{rx,n,m}^{\top}\bar{\mathbf{v}}_{n,m}t\right), \bar{\mathbf{v}} = v\begin{bmatrix} \sin\theta_v\cos\phi_v \\ \sin\theta_v\sin\phi_v \\ \cos\theta_v \end{bmatrix} \tag{3.12}$$

- For LoS field term $\mathcal{F}_{u,n,m}^{\text{LoS}}$, it is stated in Equation 3.13. Note that the $d_{3\text{D}}$ is the 3-D distance between AP's transmit antenna and STA's receive antenna. The rest terms remain the same as Equation 3.7.

$$\mathcal{F}_{u,n,m}^{\text{LoS}} = \begin{bmatrix} F_{rx,u,\theta}(\theta_{\text{LoS, ZoA}}, \phi_{\text{LoS, ZoA}}) \\ F_{rx,u,\phi}(\theta_{\text{LoS, ZoA}}, \phi_{\text{LoS, ZoA}}) \end{bmatrix}^{\top} \cdot \begin{bmatrix} 1 & 0 \\ 0 & -1 \end{bmatrix} \cdot \begin{bmatrix} F_{tx,s,\theta}(\theta_{\text{LoS, ZoD}}, \phi_{\text{LoS, AoD}}) \\ F_{tx,s,\phi}(\theta_{\text{LoS, ZoD}}, \phi_{\text{LoS, AoD}}) \end{bmatrix} \cdot \exp\left(\frac{-j2\pi d_{3\text{D}}}{\lambda_0}\right) \tag{3.13}$$

3.1.5 Apply pathloss, shadowing and the channel coefficients to the input signal

To do so, design set of Finite Impulse Response (FIR) filters to filter input signal, apply pathloss and shadowing afterwards. Note that the delays are read from the profile, as scaled in Equation 3.5.

3.2 Example Results

Figure 3.2 and Figure 3.4 demonstrate a possible realization of CDL-C channel and CDL-D channel respectively. In the NLoS scenario, echoes of signal are more dominate and spread out than the LoS conditions, given the same delay spread ($16ns$).

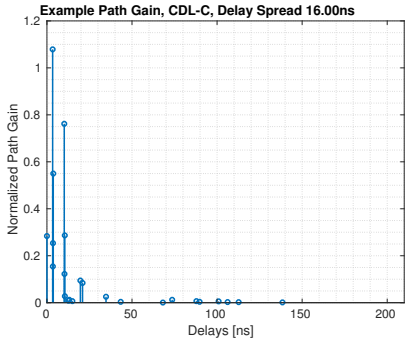

Figure 3.2: Example of CDL-C Channel (delay)

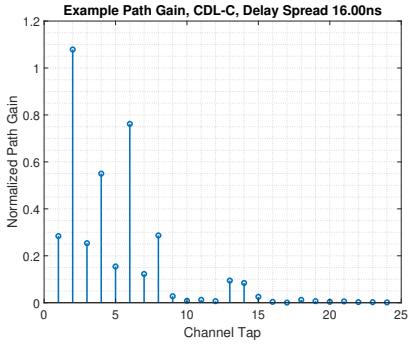

Figure 3.3: Example of CDL-C Channel (tap)

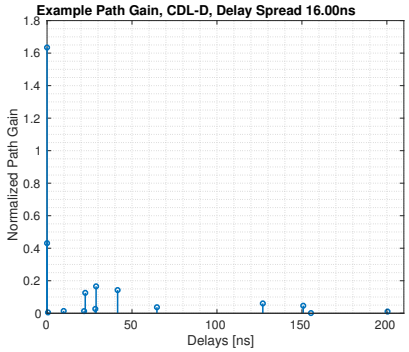

Figure 3.4: Example of CDL-D Channel (delay)

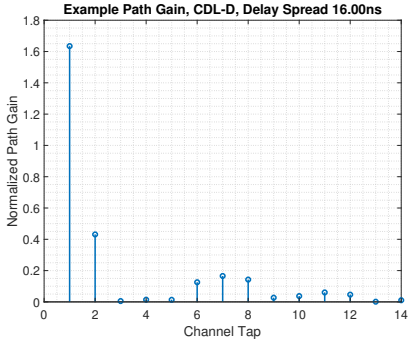

Figure 3.5: Example of CDL-D Channel (tap)

Table 3.1: CDL-C Profile (NLoS)

Cluster ID	Normalized Delay	Power [dB]	AoD [°]	AoA [°]	ZoD [°]	ZoA [°]
1	0	-4.4	-46.6	-101	97.2	87.6
2	0.2099	-1.2	-22.8	120	98.6	72.1
3	0.2219	-3.5	-22.8	120	98.6	72.1
4	0.2329	-5.2	-22.8	120	98.6	72.1
5	0.2176	-2.5	-40.7	-127.5	100.6	70.1
6	0.6366	0	0.3	170.4	99.2	75.3
7	0.6448	-2.2	0.3	170.4	99.2	75.3
8	0.656	-3.9	0.3	170.4	99.2	75.3
9	0.6584	-7.4	73.1	55.4	105.2	67.4
10	0.7935	-7.1	-64.5	66.5	95.3	63.8
11	0.8213	-10.7	80.2	-48.1	106.1	71.4
12	0.9336	-11.1	-97.1	46.9	93.5	60.5
13	1.2285	-5.1	-55.3	68.1	103.7	90.6
14	1.3083	-6.8	-64.3	-68.7	104.2	60.1
15	2.1704	-8.7	-78.5	81.5	93	61
16	2.7105	-13.2	102.7	30.7	104.2	100.7
17	4.2589	-13.9	99.2	-16.4	94.9	62.3
18	4.6003	-13.9	88.8	3.8	93.1	66.7
19	5.4902	-15.8	-101.9	-13.7	92.2	52.9
20	5.6077	-17.1	92.2	9.7	106.7	61.8
21	6.3065	-16	93.3	5.6	93	51.9
22	6.6374	-15.7	106.6	0.7	92.9	61.7
23	7.0427	-21.6	119.5	-21.9	105.2	58
24	8.6523	-22.8	-123.8	33.6	107.8	57
Per-Cluster Parameters						
Parameter		$c_{\text{ASD}}[^\circ]$	$c_{\text{ASA}}[^\circ]$	$c_{\text{ZSD}}[^\circ]$	$c_{\text{ZSA}}[^\circ]$	XPR [dB]
Value		2	15	3	7	7

Table 3.2: CDL-D Profile (LoS)

Cluster ID	Cluster PAS	Normalized Delay	Power [dB]	AoD [°]	AoA [°]	ZoD [°]	ZoA [°]
1	Specular	0	-0.2	0	-180	98.5	81.5
	Laplacian	0	-13.5	0	-180	98.5	81.5
2	Laplacian	0.035	-18.8	89.2	89.2	85.5	86.9
3	Laplacian	0.612	-21	89.2	89.2	85.5	86.9
4	Laplacian	1.363	-22.8	89.2	89.2	85.5	86.9
5	Laplacian	1.405	-17.9	13	163	97.5	79.4
6	Laplacian	1.804	-20.1	13	163	97.5	79.4
7	Laplacian	2.596	-21.9	13	163	97.5	79.4
8	Laplacian	1.775	-22.9	34.6	-137	98.5	78.2
9	Laplacian	4.042	-27.8	-64.5	74.5	88.4	73.6
10	Laplacian	7.937	-23.6	-32.9	127.7	91.3	78.3
11	Laplacian	9.424	-24.8	52.6	-119.6	103.8	87
12	Laplacian	9.708	-30	-132.1	-9.1	80.3	70.6
13	Laplacian	12.525	-27.7	77.2	-83.8	86.5	72.9

Per-Cluster Parameters

Parameter	$c_{\text{ASD}}[^\circ]$	$c_{\text{ASA}}[^\circ]$	$c_{\text{ZSD}}[^\circ]$	$c_{\text{ZSA}}[^\circ]$	XPR [dB]
Value	5	8	3	3	11

Chapter 4

802.11ad Receiver Reference Design and Performance Analysis

The receiver structure mainly contains the following important components, sequentially,

4.1 DMG packet detection

The packet detector returns the offset (in time, delay per se) from the start of the input waveform to the start of detected preamble using a simple auto-correlation, namely, that is to say, given a received signal $v(t)$, which is a delayed version of transmitted signal $u(t)$ (note that this transmitted signal is *a priori*, which composes Golay sequences, in STF and CEF), along with channel (assuming static packet-wise) coefficient c and white Gaussian noise $w(t)$, we have,

$$v(t) = cu(t - \tau_0) + w(t), t \in T_{obs} \tag{4.1}$$

Under the Maximum Likelihood (ML) criterion and treating $c = |c|e^{j\theta}, \theta \sim U[-\pi, \pi]$, we have,

$$\begin{aligned} \hat{\tau}_0 &= \arg\min_{\tau} \int_{T_{obs}} |v(t) - cu(t-\tau)|^2 \, dt \\ &= \arg\max_{\tau} \Re\left\{ c^* \int_{T_{obs}} v(t)u^*(t-\tau)dt \right\} \\ &= \arg\max_{\tau} \left| \int_{T_{obs}} v(t)u^*(t-\tau)dt \right| \end{aligned} \tag{4.2}$$

4.2 Frequency offset estimation

It is always advantageous to separate out any frequency offset – possibly caused by relative movement or, transceiver oscillators' inaccuracy – in any communication system. In this frequency offset model we have, assuming delay synchronized,

$$v(t) = |c|e^{j\theta_0}e^{j2\pi f_d t}u(t) + w(t), t \in T_{obs} \tag{4.3}$$

Following the same ML logic and treating c's phase is uniformly distributed on $-[\pi, \pi]$, we obtain,

$$\begin{aligned}
\hat{f}_d &= \arg\min_f \int_{T_{obs}} \left| v(t) - |c|e^{j\theta_0}e^{j2\pi f_d t}u(t) \right|^2 dt \\
&= \arg\max_f \Re\left\{ e^{-j\theta_0} \int_{T_{obs}} v(t)u^*(t)e^{-j2\pi f t}dt \right\} \\
&= \arg\max_f \Re\left\{ e^{-j\theta_0} \mathcal{F}\left[v(t)u^*(t)\right] \right\} \\
&= \arg\max_f \left| \mathcal{F}\left[v(t)u^*(t)\right] \right|
\end{aligned} \tag{4.4}$$

where $\mathcal{F}[\cdot]$ represents Fourier Transform.

4.3 Channel Estimation and Equalization

After delay and frequency synchronization, channel estimation is used for following Frequency Domain Equalization (FDE). Because the summation of autocorrelations of Ga_{128} and Gb_{128} composes a Dirac delta function, therefore the channel impulse response is obtained easily by a simple correlation. Figure 4.1 shows one possible estimation results, and Figure 4.1 shows statistical performance (in Mean Squared Error (MSE)).

4.4 Receiver state machine

A typical receiver state machine is pictured in Figure 4.4. Note that this is intended for single carrier only, OFDM and Control PHY are not included in the figure. In the figure, red represents PHY operations, green stands for for MAC states.

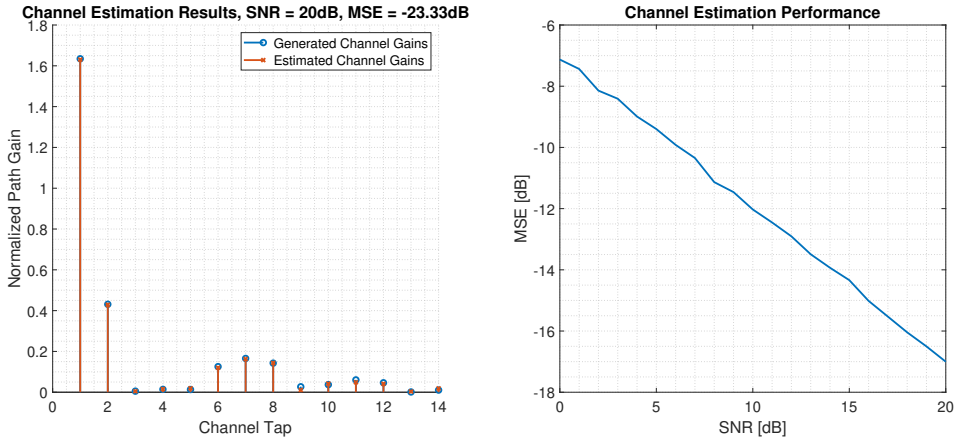

Figure 4.1: Channel Estimation Performance

4.5 PER performance of 3GPP recommended channel

The system performance of PHY transmitter-channel-receiver structure is evaluated through PER. The PER is defined as – a packet is successfully detected and no bit error in the payload part.

In the simulation, the parameters of channel is tabulated in Table 3.1 for CDL-C profile, and Table 3.2 for CDL-D profile. Except from those parameters, in the 3GPP recommended channel parameter settings, the delay spread is set to be 16 ns. System wise, according to 802.11ad protocol, the sample rate is set to be 1760 M sa/s and the carrier frequency is set to be 60.48 GHz. Besides, no Doppler shift is applied, i.e., the simulation scenario is static. Note that all scenarios are simulated under 1000 packets transmission for statistical stability.

Comparing Figure 4.3 and Figure 4.4, it can be observed that CDL-C (NLoS) conditions are worse in performance than CDL-D (LoS) conditions. For example under 10dB SNR, the PER of MCS 12 is around 10% in CDL-D whereas 100% in CDL-C. This is because the NLoS scenario has more MPC, as indicated in Figure 3.2, and those MPC tend to dominate (and resonate) on the receiver side. One can also observe that with SNR rising, the SNR is decreasing because less noise is introduced in system. Under the same SNR, lower MCS tends to be more robust than the higher ones, which is determined by modulation method and code rate.

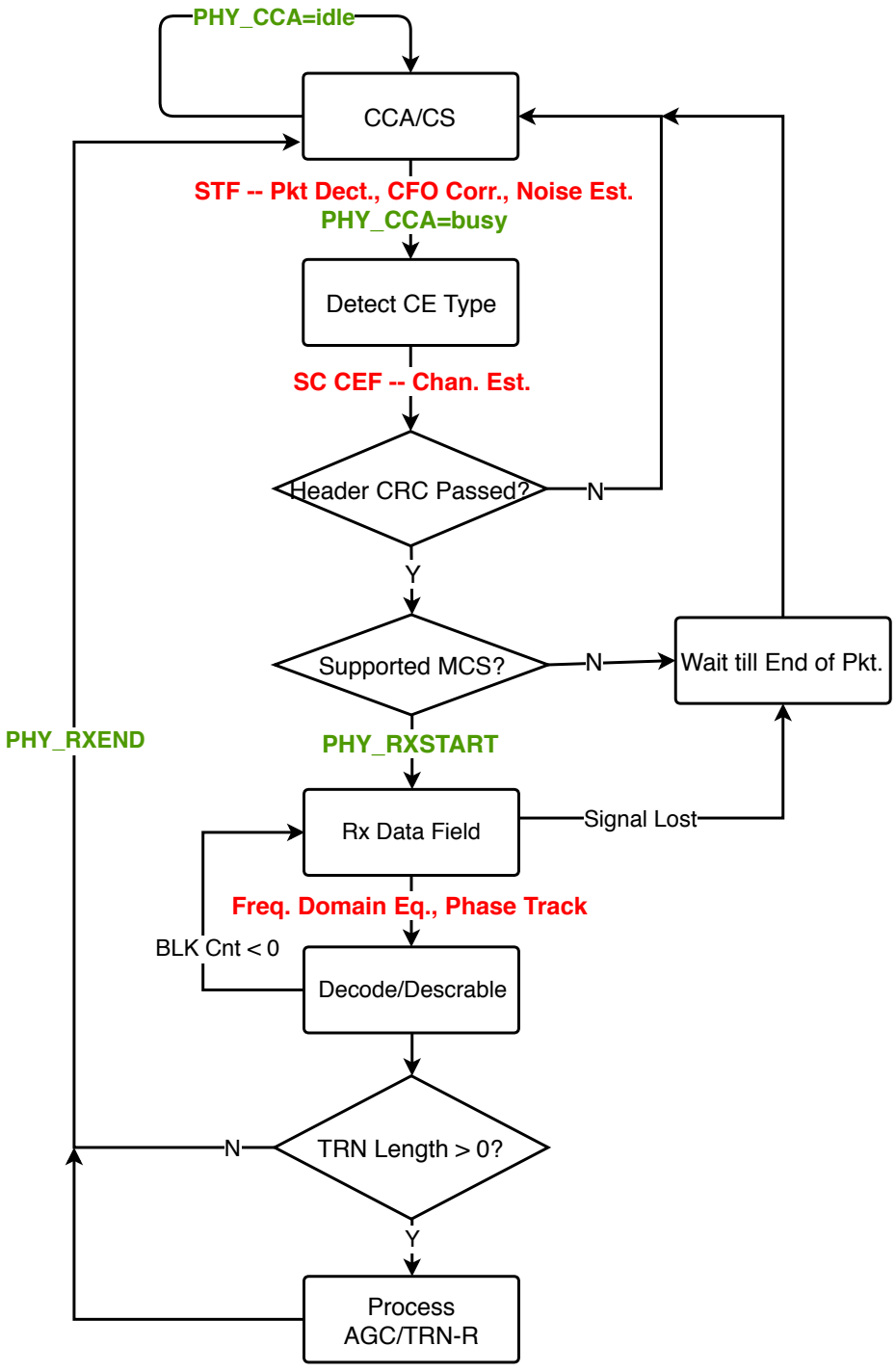

Figure 4.2: Receiver State Machine

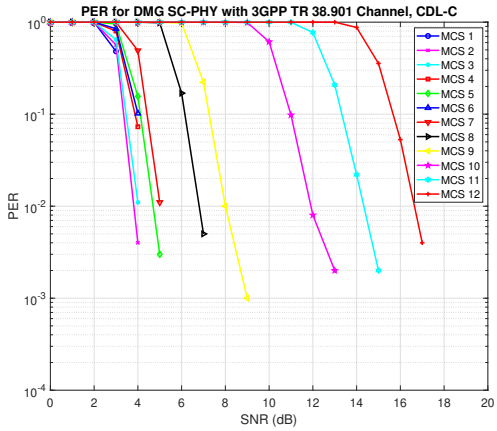

Figure 4.3: PER of CDL-C (NLoS) Profile

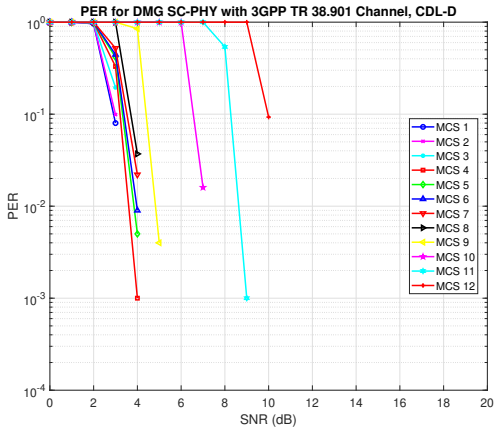

Figure 4.4: PER of CDL-D (LoS) Profile

4.6 MCS selection mechanism

To ensure timing, latency and throughput requirements from upper layer, the PHY layer should have an MCS selection mechanism to adaptively switch MCS, given certain SNR. From Figure 4.3, a Look Up Table (LUT) method can be employed here – given a measured Received Signal Strength (RSS) level and noise figure estimation, the receiver can deduct SNR value and from that SNR the receiver can further obtain pre-calculated PER.

Algorithm 1 Adaptive MCS selection

Data: SNR-PER table **t**, PER threshold th, SNR value SNR

Result: $MCS_{desired}$

$SNR_{round} = \lfloor SNR \rfloor$

for $i \leftarrow 12$ **to** $MCS = 1$ **do**

  if $t_{SNR_{round},i} \leq th$ **then**

    $MCS_{desired} = t_{SNR_{round},i}$

end

Chapter 5

Introduction to Beamforming

5.1 What is beamforming?

The first attempt to automatically localize signal sources using antenna arrays was through beamforming techniques. The idea is to *steer* array in one direction at a time and measure the output power. The steering locations which result in maximum power yield the Direction of Arrival (DoA) estimations.

The *array response* is steered by forming a linear combination of the sensor outputs,

$$y(t) = \sum_{l=1}^{L} w_l^* x_l(t) = \mathbf{w}^H \mathbf{x}(t) \tag{5.1}$$

Given samples $y(1), y(2), \cdots, y(N)$, the output power is measured by,

$$P(\mathbf{w}) = \frac{1}{N} \sum_{t=1}^{N} |y(t)|^2 = \frac{1}{N} \sum_{t=1}^{N} \mathbf{w}^H \mathbf{x}(t) \mathbf{x}^H(t) \mathbf{w} \tag{5.2}$$

Essentially, different beamforming approaches correspond to different choices of the weighting vector $\mathbf{w}$. The weight vector applied to every antenna element can be interpreted as a spatial filter, who equalize the delays (and perhaps attenuations as well) experienced by the signal on various sensors to maximally combine their respective contributions.

5.2 Bartlett's Beamformer (Conventional)

The Bartlett beamformer [11] *essentially maximizes the power of the beamforming output for a given input signal at certain direction θ.* Suppose a signal measured at the array output is given

by,

$$\mathbf{x}(t) = \mathbf{a}(\theta)s(t) + \mathbf{n}(t) \tag{5.3}$$

In Equation 5.3, $s(t)$ is transmit signal, $\mathbf{n}(t)$ is spatially white noise (uncorrelated between elements), and $\mathbf{a}(\theta)$ is the steering vector for zenith angle θ (assuming azimuth angle ϕ is 0). The steering vector will be elaborated in Section 6.1.2.

For example, L-elements Uniform Linear Array (ULA)'s steering vector is then represented as,

$$\mathbf{a}_{ULA}(\theta) = \begin{bmatrix} 1 & e^{j\phi} & \cdots & e^{j(L-1)\phi} \end{bmatrix}^{\top} \tag{5.4}$$

where, $\phi = -kd\cos\theta = \frac{\omega}{c}d\cos\theta$. $k \in [0, L-1]$ is the sequence number of an element, d is the element spacing, often times $\lambda/2$. The problem of maximization of the power is then written as,

$$\begin{aligned} \mathbf{w}_{BF} &= \arg\max_{\mathbf{w}} \mathbb{E}\left\{\mathbf{w}^H \mathbf{x}(t)\mathbf{x}^H(t)\mathbf{w}\right\} \\ &= \arg\max_{\mathbf{w}} \mathbf{w}^H \mathbb{E}\left\{\mathbf{x}(t)\mathbf{x}^H(t)\right\}\mathbf{w} \\ &= \arg\max_{\mathbf{w}} \left\{\mathbb{E}\left\{|s(t)|^2\right\}|\mathbf{w}^H\mathbf{a}(\theta)|^2 + \sigma^2|\mathbf{w}|^2\right\} \end{aligned} \tag{5.5}$$

Then if we constrain $|\mathbf{w}| = 1$, the resulting solution is then,

$$\mathbf{w}_{BF} = \frac{\mathbf{a}(\theta)}{\sqrt{\mathbf{a}^H(\theta)\mathbf{a}(\theta)}} \tag{5.6}$$

This conventional beamformer uses every available Degree of Freedom (DoF) to concentrate received energy along one direction.

5.3 Capon's Beamformer (MVDR)

Capon's [12] method attempts basically *minimize the power contributed by noise and any signals coming from other directions than θ, while maintaining a fixed gain in the pre-specified direction θ, distortionlessly*, mathematically,

$$\begin{aligned} &\min_{\mathbf{w}} P(\mathbf{w}) \\ s.t. &\& \mathbf{w}^H\mathbf{a}(\theta) = 1 \end{aligned} \tag{5.7}$$

where $P(\mathbf{w})$ is defined in Equation 5.2. The optimum solution is then given by,

$$\mathbf{w}_{CAP} = \frac{\hat{\mathbf{R}}^{-1}\mathbf{a}(\theta)}{\mathbf{a}(\theta)\hat{\mathbf{R}}^{-1}\mathbf{a}(\theta)} \tag{5.8}$$

where $\hat{\mathbf{R}} = \frac{1}{N}\sum_{t=1}^{N}\mathbf{x}(t)\mathbf{x}^H(t)$. Some authors would like to use $\mathbf{R_{xx}}$, yet the notion $\mathbf{S}$ also exists. This power minimization is basically sacrificing some noise suppression capability for more focused *nulling* in the directions where other sources present, i.e., reduces interference level to un-desired directions.

5.4 Frost's Beamformer (LCMV)

In the previous section, Capon's beamformer simply add constraint $\mathbf{w}^H\mathbf{a}(\theta) = 1$, what if we would like to have a set of constraints $\mathbf{C}$, whose columns are linear independent, and corresponding responses $\mathcal{G}$, a single column vector, i.e. mathematically,

$$\begin{aligned} &\min_{\mathbf{w}} P(\mathbf{w}) \\ s.t.\&&\mathbf{C}^H\mathbf{w} = \mathcal{G} \end{aligned} \tag{5.9}$$

By using Lagrangian multipliers, optimum solution by Frost [13] can be obtained by,

$$\mathbf{w}_{LCMV} = \hat{\mathbf{R}}^{-1}\mathbf{C}\left[\mathbf{C}^H\hat{\mathbf{R}}^{-1}\mathbf{C}\right]^{-1}\mathcal{G} \tag{5.10}$$

In the following sub-section, several typical (special case) constraints are introduced.

5.4.1 Distortionless Constraint

In this case, one can tell that Capon's beamformer is a subset of Frost's beamformer, or rather, Capon's beamformer's constraint $\mathbf{w}^H\mathbf{a}(\theta) = 1$ guarantees any signal propagate through θ angle is *distortionless*.

5.4.2 Directional Constraint

The general directional constraint is,

$$\mathbf{a}^H(\mathbf{\Theta}_i)\mathbf{w} = g_i, i \in [0, L-1] \tag{5.11}$$

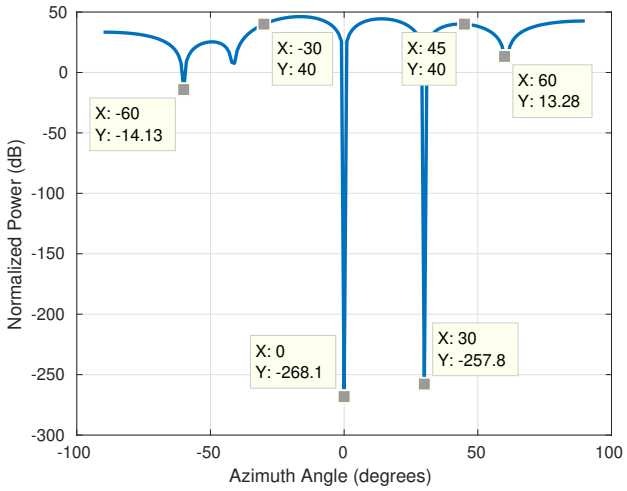

Figure 5.1: Normalized Power of LCMV beamformer with specified requirements

In this case, $\mathbf{\Theta}$ can be a vector of directions (angles). Note that $\mathbf{C} \in \mathbb{C}^{N \times M_c}$ constraint matrix is simply composed by $\mathbf{a}^H(\mathbf{\Theta}_i)$, while g_i constitutes $\mathcal{G}$.

For example, calculate the weights $\mathbf{w}$ of a 16-element ULA with,

- response of 40 dB in the direction of -30 degrees and 45 degrees azimuth,
- 0 in the direction of 0 and 30 degrees azimuth,
- and try to maintain -10 dB at direction 60 and -60 degrees.

The corresponding normalized power vs. angle plot is shown in Figure 5.1. Basically this beamformer tries to cancel out signals from 0 and 30 degrees, and keep listening on -30 and 45 degrees while guarantees the signal power level of -60 and 60 degrees stays normal.

5.4.3 Null Constraint

This type of constraint is appropriate if there is an interfering signal (jammer) coming from a known direction, that is to say,

$$\mathbf{a}^H(\mathbf{\Theta}_i)\mathbf{w}, i \in [0, L-1] \tag{5.12}$$

Chapter 6

Beamforming Enabled Massive MIMO Physical Layer Simulations

The beamforming enabled massive MIMO simulator contains the following components, namely,

1. 802.11ad PHY transmitter – which modulate the payload, prepend STF, CEF, headers, and append AGC, TRN-T/R fields
2. Phased array transmit processor – which contains a transmitter (transmits the input waveform samples with specified peak power), and a radiator (converts signals into radiated waveforms from arrays and individual sensor elements)
3. 3GPP TR 38.901 and Additive White Gaussian Noise (AWGN) channel – which impair the signal and add noise
4. Phased array receive processor – which contains a collector (collects wave fields arriving from specified direction into signals), and a receiver pre-amplifier (receives incoming signal, multiplies them by amplifier gain and divides by losses)
5. 802.11ad PHY receiver – performs synchronizations, data field abstraction and demodulation

6.1 Phased array processors – radiators, collectors, steering vectors

6.1.1 Radiators and collectors

The radiator and the collector are dual in phased array processing. Given a symbol vector contains U total symbols from PHY layer, say $\mathbf{u} \in \mathbb{C}^{S\times 1}$, the radiated signal, along with beamforming weight $\mathbf{w} \in \mathbb{C}^{M\times 1}$ assigned individually for all M elements, is given by,

$$\mathbf{y} = \mathbf{u}\mathbf{w}^H \tag{6.1}$$

$(\cdot)^H$ represents Hermitian operation.

6.1.2 Steering Vectors

Regarding the steering vector, it is defined as,

$$\mathbf{v}(\mathbf{x}, \mathbf{y}, \mathbf{z}; \alpha, \phi) = \exp\left(-j2\pi\mathbf{T}(\mathbf{x}, \mathbf{y}, \mathbf{z}; \alpha, \phi)\right) \tag{6.2}$$

where $\mathbf{T}$ is defined in Equation 6.3. $\mathbf{x}, \mathbf{y}, \mathbf{z} \in \mathbb{R}^{1\times M}$ denotes the location row vectors (in meters) for all M antenna elements and λ defines the wavelength of antenna operating center frequency.

$$\mathbf{T}(\mathbf{x}, \mathbf{y}, \mathbf{z}; \alpha, \phi) = \frac{1}{\lambda}\begin{bmatrix}\mathbf{x}\\ \mathbf{y}\\ \mathbf{z}\end{bmatrix}^{\top}\begin{bmatrix}-\cos(\alpha)\cos(\phi)\\ -\cos(\alpha)\sin(\phi)\\ -\sin(\alpha)\end{bmatrix} \tag{6.3}$$

Note that α is the elevation angle of desired steering direction, $\alpha = 90^\circ - \theta$, θ is the zenith angle. They are related to Local Coordinate System (LCS).

6.1.3 Array Response

To calculate the given array's response at certain angle (LCS), defined in α and ϕ. As illustrated in Figure 5.1, the array response operation essentially tries to read from the response plot.

$$r = \mathbf{w}^H\mathbf{v}(\mathbf{x}, \mathbf{y}, \mathbf{z}; \alpha, \phi) \tag{6.4}$$

6.2 Simulator architecture

In the beamforming enabled simulator, given a potential AP-STA pair candidateSet with total N users, their corresponding beamforming weights $\mathbf{w}$, steering vector $\mathbf{v}$. This simulator then generate an output – finalSet – indicating for individual pair, the packet go through ($True$) or not.

Algorithm 2 Beamforming enabled 802.11ad PHY with 3GPP TR 38.901 channel model simulator

Data: candidateSet, $\mathbf{w}$, $\mathbf{v}$

Result: finalSet

Initialization: finalSet $= false$

`/* Generate waveforms and responses */`

for $i \leftarrow 1$ **to** N *users* **do**
- Generate user payload, $\mathbf{s}_i$
- Generate 802.11ad PHY frame, $\mathbf{u}_i$
- Radiate waveforms, $\mathbf{y}_i = \mathbf{u}_i \mathbf{w}_i$ (Equation 6.1)
- **for** $j \leftarrow 1$ **to** N *users* **do**
  - Obtain response $r_{i,j} = \mathbf{w}_i^H \mathbf{v}_j$ (Equation 6.4)
- **end**

end

`/* Create interference, pass through channel and receive */`

for $i \leftarrow 1$ **to** N *users* **do**
- **for** $j \leftarrow 1$ **to** N *users* **do**
  - **if** j *is NOT* i **then**
    - $\mathbf{y}_i \leftarrow \mathbf{y}_i + r_{i,j} \cdot \mathbf{y}_j$
- **end**
- Pass $\mathbf{y}_i$ through channel to obtain $\mathbf{y}'_i$
- Collect waveforms to symbols $\mathbf{u}'_i$
- Demodulate and decode user payload $\mathbf{s}'_i$
- **if** $\mathbf{s}'_i$ *is* $\mathbf{s}_i$ **then**
  - finalSet$_i = True$

end

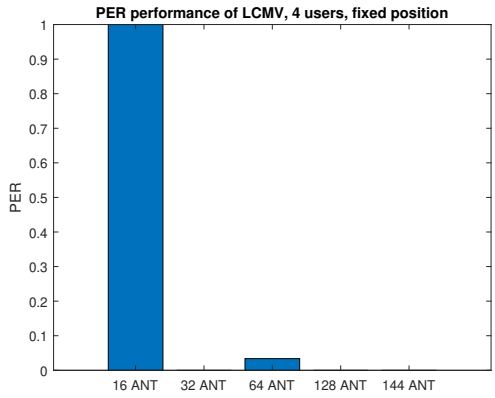

Figure 6.1: PER of LCMV beamformer with 4 users, CDL-C, fixed user position

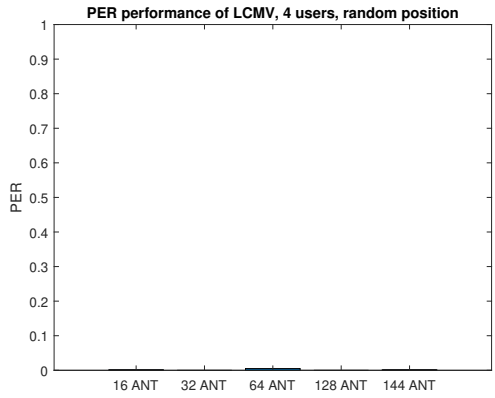

Figure 6.2: PER of LCMV beamformer with 4 users, CDL-C, random user position

6.3 Simulation Results

In the simulation, all experiments are conducted 200 packet per user per scenario, with MCS 1, and 128 bit payload length. Note also that these experiments are based on noise floor -104.5 dB, and no distance related (i.e., baseband simulation) pathloss introduced.

Figure 6.1 and Figure 6.2 demonstrate the PER performance of LCMV beamformer in the fixed user position scenario and random position user scenario, respectively. As we can observe from the plot, more antenna, the better PER performance – this is because the directivity of synthesized beam is higher when more antenna are present. The reason of random case is better than fixed case lie in that, random cases' users (which located uniformly on a unit sphere) are more dispersed than the fixed position (which located uniformly on a unit disk) – the elevation of users are non zeros in the random case. Figure 6.3 and Figure 6.4 show the PER performance of LCMV beamformer under different number of users (constrains). Clearly the trend follows, more users, more errors. Same conclusion of random case vs. fixed case still holds.

As a comparison, Figure 6.5 and 6.6 show the results of PER under heuristics beamformer, which is a genetic algorithm optimized hybrid beamforming mechanism, whose objective function is stated in Equation 6.5. As observed before, more antenna tends to have less PER, and more users, the system is prone to error.

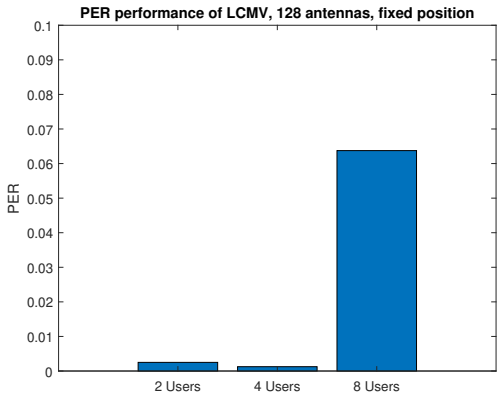

Figure 6.3: PER of LCMV beamformer with 128 antennas, CDL-C, fixed user position

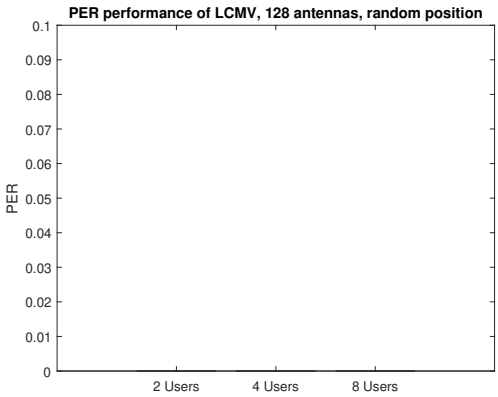

Figure 6.4: PER of LCMV beamformer with 128 antennas, CDL-C, random user position

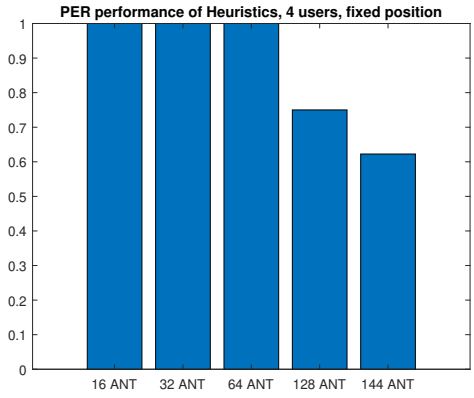

Figure 6.5: PER of heuristics beamformer with 4 users, CDL-C, fixed user position

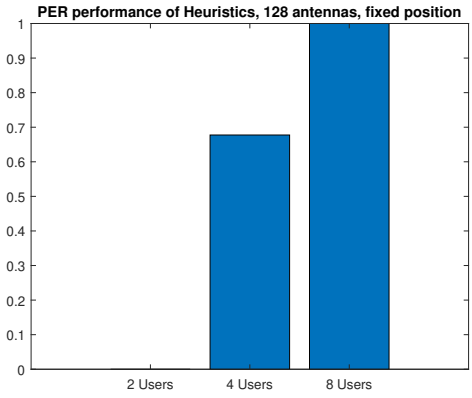

Figure 6.6: PER of heuristics beamformer with 128 antennas, CDL-C, fixed user position

$$
\begin{aligned}
\{\mathbf{F}^*_{\mathbf{RF}}, \mathbf{F}^*_{\mathbf{BB}}\} \quad &= \quad \arg\min_{\mathbf{F_{RF}},\mathbf{F_{BB}}} \quad \textstyle\sum_{\forall u \in U} \tilde{r}_u - r_u \\
s.t. \qquad & \textstyle\sum_{i=j} \left| \mathbf{F}^{*(i,j)}_{\mathbf{RF}} \right| = 1 \\
& \textstyle\sum_{\forall j} \mathbf{F}^{*(i,j)}_{\mathbf{RF}} = 1, \quad \forall i \in [1, N_{RF}] \\
& \textstyle\sum_{i=j} \mathbf{F}^{*(i,j)}_{\mathbf{BB}} = P \\
& \textstyle\sum_{i \neq j} \mathbf{F}^{*(i,j)}_{\mathbf{BB}} = 0
\end{aligned}
\tag{6.5}
$$

Note that $\mathbf{F}^*_{\mathbf{RF}}, \mathbf{F}^*_{\mathbf{BB}}$ is the analog phase shifter weight and digital baseband precoder, respectively, $\mathbf{W} = \mathbf{F_{BB}}\mathbf{F_{RF}}$. $\tilde{r}_u$ is the actual throughput for user u, and r_u is the desired throughput. N_{RF} is the number of RF chains (which is typically smaller than number of antenna in hybrid beamforming system).

Chapter 7

Conclusion

With the growth of data traffic in cellular networks, and more demanding requirements, traditional sub 6GHz system capacities are prone to reach their maximum. Millimeter wave communications are emerging recently, with its advantages in higher bandwidth and throughput, gradually adapted in next generation of communications.

However, mmWave communication will need to overcome the exponentially growth of pathloss caused by ten-folds on center frequency. Combining beamforming, massive MIMO technology with mmWave communication is promising given its small wavelength. This thesis present a massive MIMO mmWave communication link simulator design by presenting 802.11ad PHY layer specification and its reference receiver design, along with introduction and application of 3GPP TR 38.901 channel model and beamforming enabled simulator design.

Simulation results of the proposed integrated simulator demonstrate its potential of aiding quantification of different beamforming techniques performance through PER, a critical PHY layer metric. Generally speaking, the simulator shows that the more antenna a system poses, the better PER performance; whereas more user, poorer PER.

Regarding its contribution, this beamforming-communication simulator also enables the development of MAC layer on top of PHY, by examining the validity of state machines, under highly directional radio link which differentiate mmWave with traditional sub-6 GHz communication protocol design – Carrier Sensing (CA) and Clear Channel Assessment (CCA) may no longer needed or need to be revolutionized.

Bibliography

[1] T. S. Rappaport, S. Sun, R. Mayzus, H. Zhao, Y. Azar, K. Wang, G. N. Wong, J. K. Schulz, M. Samimi, and F. Gutierrez, "Millimeter wave mobile communications for 5g cellular: It will work!" *IEEE access*, vol. 1, pp. 335–349, 2013.

[2] W. Roh, J.-Y. Seol, J. Park, B. Lee, J. Lee, Y. Kim, J. Cho, K. Cheun, and F. Aryanfar, "Millimeter-wave beamforming as an enabling technology for 5g cellular communications: Theoretical feasibility and prototype results," *IEEE communications magazine*, vol. 52, no. 2, pp. 106–113, 2014.

[3] S. Sun, T. S. Rappaport, R. W. Heath, A. Nix, and S. Rangan, "Mimo for millimeter-wave wireless communications: Beamforming, spatial multiplexing, or both?" *IEEE Communications Magazine*, vol. 52, no. 12, pp. 110–121, 2014.

[4] O. El Ayach, S. Rajagopal, S. Abu-Surra, Z. Pi, and R. W. Heath, "Spatially sparse precoding in millimeter wave mimo systems," *IEEE transactions on wireless communications*, vol. 13, no. 3, pp. 1499–1513, 2014.

[5] Z. Pi and F. Khan, "An introduction to millimeter-wave mobile broadband systems," *IEEE communications magazine*, vol. 49, no. 6, 2011.

[6] A. Natarajan, S. K. Reynolds, M.-D. Tsai, S. T. Nicolson, J.-H. C. Zhan, D. G. Kam, D. Liu, Y.-L. O. Huang, A. Valdes-Garcia, and B. A. Floyd, "A fully-integrated 16-element phased-array receiver in sige bicmos for 60-ghz communications," *IEEE Journal of Solid-State Circuits*, vol. 46, no. 5, pp. 1059–1075, 2011.

[7] S. Sanayei and A. Nosratinia, "Antenna selection in mimo systems," *IEEE Communications Magazine*, vol. 42, no. 10, pp. 68–73, 2004.

[8] A. F. Molisch, M. Z. Win, Y.-S. Choi, and J. H. Winters, "Capacity of mimo systems with antenna selection," *IEEE Transactions on Wireless Communications*, vol. 4, no. 4, pp. 1759–1772, 2005.

[9] "Wireless LAN Medium Access Control (MAC) and Physical Layer (PHY) Specifications Amendment 3: Enhancements for Very High Throughput in the 60 GHz Band," *IEEE Std. 802.11ad*, 2012.

[10] 3GPP, "5g; study on channel model for frequencies from 0.5 to 100 ghz," 3rd Generation Partnership Project (3GPP), Tech. Rep. 38.901, 2017.

[11] M. Babtlett, "Smoothing periodograms from time-series with continuous spectra," *Nature*, vol. 161, no. 4096, p. 686, 1948.

[12] J. Capon, "High-resolution frequency-wavenumber spectrum analysis," *Proceedings of the IEEE*, vol. 57, no. 8, pp. 1408–1418, 1969.

[13] O. L. Frost, "An algorithm for linearly constrained adaptive array processing," *Proceedings of the IEEE*, vol. 60, no. 8, pp. 926–935, 1972.